Anomalous Diffusion Due to Binding: A Monte Carlo Study

Michael J. Saxton
Institute of Theoretical Dynamics, University of California, Davis, California 95616, and Laboratory of Chemical Biodynamics, Lawrence Berkeley National Laboratory, University of California, Berkeley, California 94720 USA

ABSTRACT In classical diffusion, the mean-square displacement increases linearly with time. But in the presence of obstacles or binding sites, anomalous diffusion may occur, in which the mean-square displacement is proportional to a nonintegral power of time for some or all times. Anomalous diffusion is discussed for various models of binding, including an obstruction/binding model in which immobile membrane proteins are represented by obstacles that bind diffusing particles in nearest-neighbor sites. The classification of binding models is considered, including the distinction between valley and mountain models and the distinction between singular and nonsingular distributions of binding energies. Anomalous diffusion is sensitive to the initial conditions of the measurement. In valley models, diffusion is anomalous if the diffusing particles start at random positions but normal if the particles start at thermal equilibrium positions. Thermal equilibration leads to normal diffusion, or to diffusion as normal as the obstacles allow.

INTRODUCTION

In unobstructed diffusion, the mean-square displacement of the diffusing particle is proportional to time. But obstruction or binding may lead to anomalous diffusion, in which diffusion is hindered and the mean-square displacement is proportional to a fractional power of time less than one (Bouchaud and Georges, 1988, 1990; Haus and Kehr, 1987; Havlin and Ben-Avraham, 1987; Scher et al., 1991). In earlier work (Saxton, 1994) we considered obstruction by inert obstacles; here we treat several models of binding.

Anomalous diffusion has been reported in single-particle tracking experiments on the low-density lipoprotein (LDL) receptor on human skin fibroblasts (Ghosh, 1991), single-particle tracking experiments on a neural cell adhesion molecule in muscle cells (Simson, 1994), and fluorescence photobleaching recovery experiments on IgE receptors in rat basophilic leukemia cells (Brust-Mascher et al., 1993; Feder, 1993). Anomalous diffusion in cell membranes may depend on metabolic energy; in the fibroblast experiments, the fraction of receptors showing anomalous diffusion decreased on treatment with azide and deoxyglucose (Ghosh, 1991). Nagle (1992) showed that long-time tails in the waiting time have a major effect on fluorescence photobleaching recovery. Both the diffusion coefficient and the fractional recovery may depend on the measurement time.

To what extent can binding be responsible for anomalous diffusion in cell membranes? We examine several models. Pure obstruction by inert random point obstacles is considered, to make contact with previous work and to serve as a reference system. In the obstruction/binding model, point obstacles, representing immobile membrane proteins, bind tracers in nearest-neighbor sites, as in the "post model" of Jacobson and co-workers (Zhang et al., 1993). We also consider a site diffusion model with a singular distribution of binding energies, two bond diffusion models with different distributions of barrier heights, and the continuous-time random walk model used by Nagle (1992).

METHODS

Diffusion calculations are carried out by modifications of the method used earlier (Saxton, 1987, 1992). Immobile point obstacles are placed on a triangular lattice at random at a prescribed concentration. A tracer is placed at a random unblocked point on the lattice and carries out a random walk on unobstructed lattice sites. The tracer position is recorded as a function of time, and the mean-square displacement $\langle r^2 \rangle$ is obtained by averaging the positions over different random walks with the same configuration of obstacles or traps, and different configurations with the same area fraction of obstacles or statistical distribution of traps. Typically, 50 different configurations were used, with 200 random walks per configuration. In each run, at least 256K time steps were used (1K = 1024). Periodic boundary conditions were imposed, and unless otherwise specified, a 256 × 256 lattice was used. The approximations involved in a lattice model of lateral diffusion are discussed elsewhere (Scalettar and Abney, 1991; Saxton, 1993a, 1994).

In the valley models, each lattice point is assigned a well depth depending on the model used. In the mountain models, each bond connecting nearest-neighbor sites is assigned a barrier height from a prescribed probability distribution. The random walk is carried out using the Metropolis Monte Carlo algorithm (Binder and Heermann, 1992). In general, the transition probability in the Metropolis algorithm is

$$W = \begin{cases} 1 & E_F \le E_I \\ \exp[-\beta(E_F - E_I)] & E_F > E_I, \end{cases} \quad (1)$$

where E_I is the energy of the initial state, E_F is the energy of the final state, $\beta = 1/kT$, k is the Boltzmann constant, and

Received for publication 12 October 1995 and in final form 12 December 1995.

Address reprint requests to Dr. Michael J. Saxton, Institute of Theoretical Dynamics, University of California, Davis, CA 95616-8618. Tel.: 916-752-6163; Fax: 916-752-7297; E-mail: mjsaxton@ucdavis.edu.

0006-3495/96/03/1250/13 $2.00

T is temperature. A random number R between 0 and 1 is generated. If $R \leq W$, the tracer is moved; otherwise it remains. In either case the clock is incremented by one time step.

We assume short-range binding forces, so that the probability of a move depends only on a single energy, the well depth in valley models or the barrier height in mountain models (see, for example, Mak et al., 1988). For long-range binding forces, a tracer at a given site interacts with adjacent sites and the transition probability depends on the difference in energies between initial and final positions (see, for example, Jiang and Metiu, 1988).

The choice of initial position for a tracer is important, and three different methods were used. In the first, the initial position is simply a random unblocked site. In the second, a tracer is placed at a random unblocked site and allowed to carry out a random walk for a prescribed annealing time. The mean-square displacement is not recorded during this time, and the position of the tracer at the end of this time is taken to be its initial position. Then the tracer continues its random walk and its mean-square displacement is recorded as a function of time. In the limit of infinite annealing time, the initial position of the tracer is its thermal equilibrium position. In the third method, the initial position is chosen from the thermal equilibrium distribution. If the energy of the ith site is $-|E_i|$, then the probability of escape is $W_i = \exp(-\beta|E_i|)$ and the waiting time is $t_i = 1/W_i$. The equilibrium probability that a tracer will be at site i is then

$$P_i = \frac{t_i}{\sum_j t_j} = \frac{\exp(+\beta|E_i|)}{\sum_j \exp(+\beta|E_j|)}, \tag{2}$$

where the sum is over all sites.

For the case of the power law distribution, each site has a different probability, and the following algorithm was used. For a given configuration of binding sites, go through the lattice points in numerical order and calculate the normalized cumulative distribution $\phi(n) = \sum_{i=1}^{n} P_i$. Then, at the start of each random walk, choose a random number R between 0 and 1, find n such that $\phi(n) \leq R \leq \phi(n+1)$, and choose site n as the initial site. To see that this works, note that if all the P_i's are equal, each point has an equal probability of being chosen as the initial site. If one point is a very deep well, P_i is large there, ϕ makes a large jump there, and that point has a high probability of being chosen as the initial site.

Some complications in time-dependent Monte Carlo models with binding have been discussed in the context of diffusion of an adsorbed atom on a surface (review: Kang and Weinberg, 1992). The principle of detailed balance does not specify the transition probabilities uniquely, and the time course of the model depends on the choice of transition probabilities. For the relation between simulated time and real time to be well defined, the transition probabilities must be based on activation energies, not on the energy differences between initial and final states (Kang and Weinberg, 1992). If the activation barrier between initial and final states is negligible, the Kang-Weinberg transition probabilities reduce to the Metropolis probabilities.

To convert the dimensionless units r^* and t^* used in the Monte Carlo calculations to experimental units r and t, we use the lattice constant ℓ as the unit of length, the jump time τ as the unit of time, and D_0 as the diffusion coefficient of the tracer in an unobstructed system. The obstacle concentration C is the area fraction, defined as the fraction of lattice points occupied by obstacles, and $\{W\}$ is the set of escape probabilities. Then $r = \ell r^*$, $t = \tau t^*$, $D = D_0 D^*(C,\{W\})$ with $D^*(0,\{1\}) = 1$, and $\ell^2 = 4D_0\tau$. The basic relation $\langle r^2 \rangle = 4Dt$ yields $\langle r^{*2} \rangle = D^*(C,\{W\})\, t^*$, and for anomalous diffusion $\langle r^{*2} \rangle = D^*(C,\{W\})\, t^{*2/d_w}$. We take ℓ to be (infinitesimally less than) the sum of the diameters of an obstacle and a tracer, so that a pair of adjacent obstacles will just block passage of a tracer between them. Then τ is the time required for a tracer to diffuse a mean-square distance of ℓ^2 in the unobstructed system. The modification to τ required for systems with binding or hydrodynamic interactions will be discussed later. The escape rate from a binding site is W/τ in physical units. To simplify the notation, we drop the asterisks from r and t, except in the discussion of experimental results.

RESULTS

We begin with a discussion of some guiding principles, lest we get lost in a maze of trap models. Foremost is the distinction between normal and anomalous diffusion. In most of the cases examined, diffusion is anomalous at short times and normal at long times. Second is the distinction between valley and mountain models. Third, the initial conditions for the diffusion measurement may determine whether diffusion is normal or anomalous. Finally, we consider singular versus nonsingular distributions of waiting times.

In general, why can diffusion be anomalous? A change in the law of Brownian motion implies a breakdown in the central limit theorem. The central limit theorem requires that the variables must not be distributed too broadly and the correlations must not be too long-range. So anomalous diffusion may result from a pathological distribution of variables—a broad distribution of jump lengths or jump times—or from long-range correlations in the elementary displacements (Bouchaud and Georges, 1988, 1990).

Anomalous diffusion: nonbinding point obstacles

To demonstrate the method of data analysis and to provide a reference system, we first consider point obstacles without binding. In normal diffusion, the mean-square displacement $\langle r^2 \rangle$ is given by

$$\langle r^2 \rangle = 4Dt \tag{3}$$

and in anomalous diffusion

$$\langle r^2 \rangle \sim t^{2/d_w}, \tag{4}$$

where D is the diffusion coefficient, t is time, and d_w is the anomalous diffusion exponent. In the cases considered here, diffusion is hindered and $d_w \geq 2$. In the presence of obstacles, diffusion is anomalous at short times and normal at long times. The transition between these two regions occurs at the crossover time t_{CR}; the corresponding distance is the crossover length

$$R_{CR} = \sqrt{D^*(C)t_{CR}}, \tag{5}$$

where $D^*(C)$ is the diffusion coefficient for long times. So we have

$$\langle r^2 \rangle \sim \begin{cases} t^{2/d_w} & t \ll t_{CR} \\ t & t \gg t_{CR} \end{cases}. \tag{6}$$

A conventional plot of $\langle r^2 \rangle$ versus t does not show this structure clearly. It is useful to remove the asymptotic linear time dependence and plot the Monte Carlo results as $\log[\langle r^2 \rangle / t]$ versus $\log t$. The region of anomalous diffusion then yields a straight line with slope $2/d_w - 1$, and the region of normal diffusion yields a horizontal line. The intersection of these two lines gives the crossover time, and the value of $\langle r^2 \rangle / t$ in the region of normal diffusion is $D^*(C)$. With this plot, it is easy to see whether a Monte Carlo run was long enough for D^* to have reached its asymptotic value (Saxton, 1994).

Anomalous diffusion is thus characterized by three parameters, the anomalous diffusion exponent d_w, the crossover time t_{CR}, and the long-range diffusion coefficient $D^*(C)$. The steeper the slope in the anomalous region, the larger d_w is.

The method of analysis is shown in Fig. 1 for diffusion in the presence of inert point obstacles, that is, obstacles that do not bind the diffusing species. As the concentration of obstacles increases, diffusion becomes more anomalous over longer times—d_w and t_{CR} both increase. At the percolation threshold C_P, $t_{CR} \to \infty$, and diffusion is always anomalous. At the percolation threshold, the diffusion coefficient goes to zero in the limit of an infinite system.

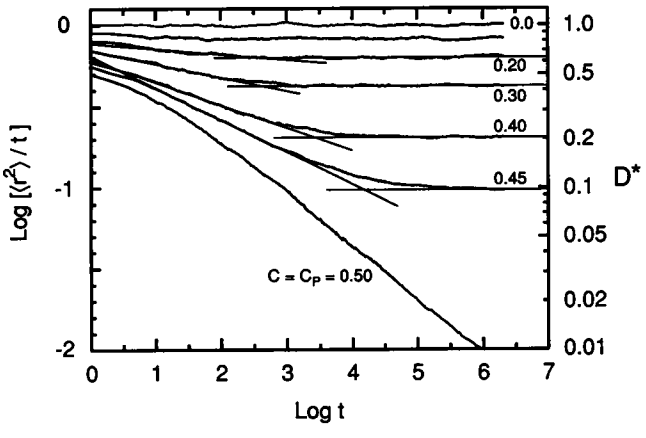

FIGURE 1 Anomalous diffusion of a point tracer on a triangular lattice in the presence of inert point obstacles at the indicated obstacle concentrations C (Saxton, 1994). Monte Carlo results for the mean-square displacement $\langle r^2 \rangle$ are plotted as $\log[\langle r^2 \rangle / t]$ versus $\log t$. The horizontal lines are the average value of $\log[\langle r^2 \rangle / t]$ for large t. The slanted lines are least-squares fits of a straight line to the Monte Carlo results for small t; the slopes yield d_w. The intersection of the two lines defines the crossover time t_{CR}. The percolation threshold for the triangular lattice is $C_P = 0.5$.

Mountain and valley models

One must distinguish between valley models and mountain models (Fig. 2 *a*). In a valley model, each lattice site is assigned a well depth from a prescribed statistical distribution, and a tracer must reach the $E = 0$ level to be able to move. When a tracer tries to move, it knows how deep a hole it is trying to escape but not how deep a hole it is entering, and it has an equal probability of moving in any direction to escape. The probability of escape from the ith site is $W_i = \exp(-\beta|E_i|)$, and the average waiting time is $\tau_i = \exp(+\beta|E_i|)$, where $\beta = 1/kT$. Note that throughout the paper we vary energy at constant temperature.

The mountain model is a bond diffusion model in which all sites are identical, with $E = 0$, but adjacent sites are joined by bonds with prescribed barrier heights. The transition probability from site i to site j is $W_{ij} = \exp(-\beta E_{ij})$, where E_{ij} is the barrier height between sites i and j. The bonds at a particular site may have different transition probabilities, but $W_{ij} = W_{ji}$.

A high barrier in the mountain model has much less effect than a deep well does in the valley model, because in the mountain model a tracer is likely to take an alternative route around a high barrier, except in the one-dimensional case (Bunde, 1988).

One could combine these models and assume the energies of lattice sites and barriers are both randomly distributed. A version of this model is discussed by Limoge and Bocquet (1991).

Fig. 2 *b* shows a particular valley model we shall consider, the obstruction/binding model. Here obstacles bind tracers occupying nearest-neighbor sites. In the uniform obstruction/binding model, the well depth is $-|\Delta E|$ for an unblocked site adjacent to one or more obstacles, and 0 for all other sites. In the variable obstruction/binding model, each nearest-neighbor obstacle contributes an equal binding energy, so that a site with n nearest-neighbor obstacles has a well depth of $-n|\Delta E|$. These are forms of the post model (Zhang et al., 1993). All obstacles are assumed to bind tracers, but in a cell membrane not all immobile species necessarily bind all mobile species.

In the valley model, we assume a short-range interaction, that is, the range of the binding energy is much shorter than the spacing between adjacent obstacles. As discussed in Methods, the energy change in a move then depends only on the energy at the initial site. To be able to move, a tracer must have enough thermal energy to reach $E = 0$. The physical picture is that at each move the tracer escapes from the initial binding site, diffuses, and is then bound at the final site. To make clear what will not be discussed here, a

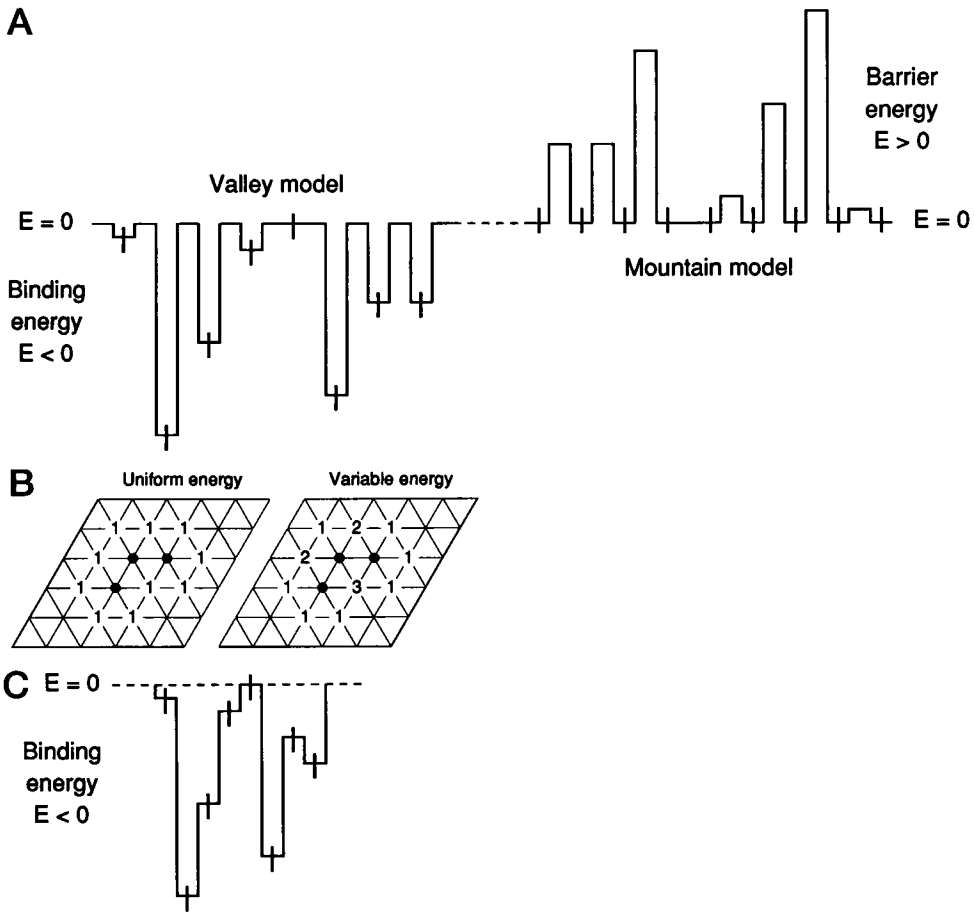

FIGURE 2 (*A*) Energy levels in the valley and mountain models with short-range interactions. Vertical ticks indicate lattice sites. (*B*) The obstruction/binding model. Obstacles (●) bind tracers occupying nearest-neighbor sites. Relative binding energies for the nearest-neighbor sites are shown. (*C*) The valley model with a long-range interaction, which will not be considered here.

long-range interaction model is shown in Fig. 2 *c* for the valley model. Here the probability of escape depends on the energy difference between initial and final states. The dependence of the diffusion coefficient on the obstacle concentration is complex, because diffusion is facilitated at the percolation threshold of binding sites. In the uniform obstruction/binding model, for example, a tracer could diffuse along the interface with no change in binding energy (Parris and Bookout, 1993).

Initial conditions

At first glance, the initial condition for the Monte Carlo calculations appears to be a purely technical matter that belongs in Methods, but it is essential to understanding when anomalous diffusion occurs. For some models a random initial condition leads to anomalous diffusion (Harder et al., 1987), but a thermal equilibrium initial condition leads to normal diffusion (Haus and Kehr, 1987).

In a system with inert obstacles, the initial position of a tracer is simply a random unblocked site. Similarly, in a mountain model, all lattice sites are at an energy $E = 0$, and the initial position is a random site. But in a valley model, there are several ways of choosing the initial position. First, the initial position may be random. This is a nonequilibrium state because the probability of starting at any unblocked site is uniform, independent of the well depth at that site. Second, the initial position may be chosen from the thermal equilibrium distribution (Eq. 2), so that a tracer is more likely to start in the deeper wells. Third, the initial position can be found by annealing. Here the tracer starts at a random unblocked site and carries out a random walk for a prescribed annealing time. Its position at the end of the annealing time is taken to be the initial position, and then the tracer continues the random walk and its mean-square displacement is recorded. This method interpolates between the others.

For a valley model, if the initial position of the tracer is given by a thermal equilibrium distribution, diffusion is normal at all times, and the diffusion coefficient is known exactly:

$$D^* = \langle 1/W \rangle^{-1}. \tag{7}$$

Here W is the probability of escape, and the average is over all sites (Haus and Kehr, 1987).

As shown in Fig. 3, annealing has no effect on diffusion in the presence of inert obstacles. But for the variable obstruction/binding model, the nature of the diffusion is determined by the initial state. For a random initial condition, diffusion is anomalous. For an equilibrium initial condition, diffusion is normal. For a random initial distribution

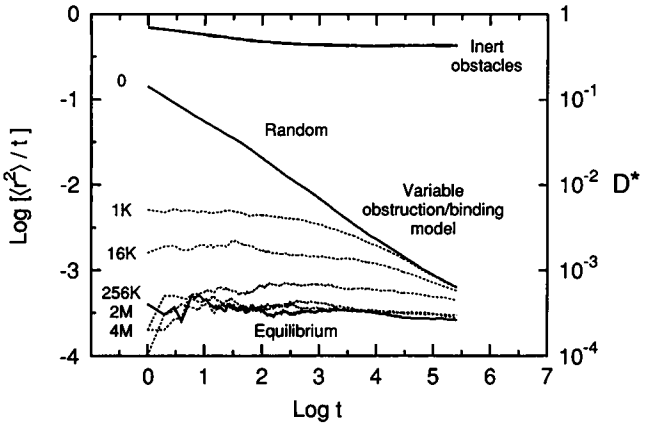

FIGURE 3 The effect of initial conditions on lateral diffusion. (*Upper curves*) Inert random point obstacles at an area fraction $C = 0.3$, for random initial conditions and annealing times of 16K and 256K (1K = 1024, 1 M = 1024^2). Annealing has no effect on diffusion. (*Lower curves*) Variable obstruction/binding model for $C = 0.3$ and the indicated annealing times. Here the well depth is $2.3kT$, so that the escape probability from a binding site with one adjacent obstacle is $W = 0.1$. For random initial conditions, diffusion is anomalous at all times shown; for equilibrium initial conditions, diffusion is normal at all times. For moderate annealing times (1K, 16K), diffusion is normal initially and becomes anomalous at large times. Long annealing times (≥2 M) are required to reach equilibrium.

with annealing, diffusion shifts from anomalous to normal as the annealing time increases.

The strong dependence on initial conditions may be less surprising in view of work on reaction kinetics in low-dimensional systems. In the rate law for the $A + B \rightarrow 0$ reaction, for example, the exponent of time is different for correlated and uncorrelated initial conditions (Lindenberg et al., 1989, 1990).

What does this dependence imply for measurements of diffusion? In an ideal diffusion experiment, the label has no effect on the tracer, and the tracer has time to reach its thermal equilibrium distribution. A pulsed-gradient spin-echo NMR measurement is practically ideal; a photobleaching experiment is ideal if the interaction of the tracer with the obstacles is the same for the bleached and unbleached forms. But if photobleaching affects the interaction of tracers and binding sites significantly, the tracer will be in a nonequilibrium distribution. An example of an ideal nonequilibrium initial distribution is photogeneration of electron-hole pairs in a solid (Scher et al., 1991).

Singular distributions

A final distinction involves the distribution of escape probabilities (Harder et al., 1987; Haus and Kehr, 1987). In a singular distribution, there is a nonzero probability of obtaining any escape probability $W > 0$, however small, or equivalently any waiting time, however large. In a nonsingular distribution, W cannot be arbitrarily small. For Eq. 7 to hold, the distribution of escape probabilities must be nonsingular so that the system can be in thermal equilibrium. For a singular distribution, the system size is important because the larger the system, the greater the chance of an extremely small value of W.

Equilibrium constants

Binding is described here in terms of energies, but it can also be expressed in terms of equilibrium constants. For a binding site of energy $|\Delta E|$, the equilibrium constant is

$$K = K_0 \exp[-|\Delta E|/kT]. \quad (8)$$

To evaluate K_0, it is necessary to assume more details of the structure of the species and the potential energy of the interaction. In order to construct vibrational and rotational partition functions. Such a derivation is carried out in detail in Hill (1985).

Binding models

We examine several binding models. We have already discussed the reference system, point obstacles without binding. First, we consider the most biological model, the obstruction/binding model with uniform and nonuniform well depths. Next, we examine point binding sites with a power law distribution of well depths to see the effect of a singular distribution. Then we look at two bond diffusion models as examples of the mountain model. Finally, we consider a continuous-time random walk (CTRW) model with a singular distribution of waiting times, as used by Nagle (1992). We then summarize the results in terms of the diffusion coefficients and discuss experimental results on the LDL receptor.

Obstruction/binding model: uniform binding energies

A plausible model of a cell membrane combines obstruction and binding. Point obstacles, representing immobile proteins, are placed at random sites on a lattice. Moves to sites occupied by obstacles are forbidden, and the obstacles bind tracers in nearest-neighbor sites.

In the uniform binding model, if a site is adjacent to one or more obstacles, the well depth is $-|\Delta E|$, and if not, the well depth is 0. The escape probability from a binding site to any unblocked site is $W = \exp(-\beta|\Delta E|)$, independent of the energy of the destination.

Fig. 4 shows results for the uniform obstruction/binding model for various escape probabilities W. For $C = 0.1$ and random initial conditions (Fig. 4 *a*), diffusion is anomalous at short times, much more anomalous than in the case of inert obstacles, as shown by the steep slope. At long times, diffusion becomes normal. For thermal equilibrium initial conditions, as the escape probability decreases, the diffusion coefficient decreases but the pattern of anomalous diffusion is the same as for inert obstacles. For $C = 0.3$ and thermal

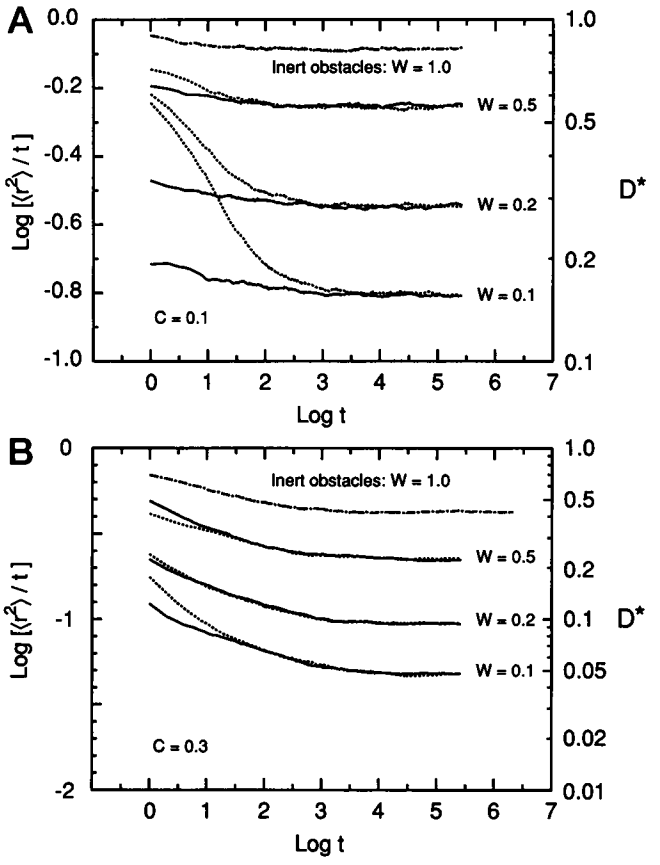

FIGURE 4 Uniform obstruction/binding model. Log[$\langle r^2\rangle/t$] as a function of log t, for the indicated escape probabilities W and an area fraction of obstacles C. (*A*) $C = 0.1$. (*B*) $C = 0.3$. – · –, Inert obstacles, $W = 1$. – – –, Random initial conditions. ——, Thermal equilibrium initial conditions. Note that $W = 0.5$ corresponds to a well depth of $0.7kT$; $W = 0.2$ to $1.6kT$; and $W = 0.1$ to $2.3kT$. At $C = 0.1$, a well depth of kT lowers D^* by a factor of 2.2, and at $C = 0.3$ by a factor of 2.5.

equilibrium initial conditions (Fig. 4 *b*), again the diffusion coefficient decreases and the pattern of anomalous diffusion is little changed. The initial conditions have little effect because most sites are binding sites at this obstacle concentration. Here 30% of the sites are obstacles, 61.8% are binding sites, and only 8.2% are nonbinding. As C goes from 0.1 to 0.2 to 0.3 to 0.4, the fraction of nonbinding sites decreases from 0.48 to 0.21 to 0.082 to 0.028. As the fraction of nonbinding sites goes to zero, diffusion becomes equivalent to diffusion in the presence of inert obstacles but with a jump rate reduced by a factor of W.

Obstruction/binding model: variable binding energies

In the variable obstruction/binding model, the well depth at a site is $-n|\Delta E|$, where n is the number of obstacles adjacent to the site. The escape probability from the site to any unblocked site is $W = \exp(-\beta n|\Delta E|)$.

Fig. 5 shows the results for $C = 0.3$, the same obstacle concentration as in Fig. 4 *b*. The diffusion coefficients

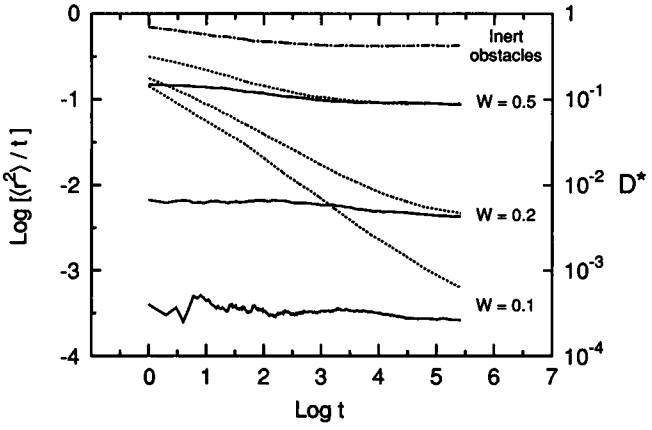

FIGURE 5 Variable obstruction/binding model. Log[$\langle r^2\rangle/t$] as a function of log t, for the indicated escape probabilities W. The area fraction of obstacles is $C = 0.3$. – · –, Inert obstacles, $W = 1$. – – –, Random initial conditions. ——, Thermal equilibrium initial conditions. Note the scale change from Fig. 4.

are much lower because there are many high-affinity binding sites. In the uniform model all binding sites have an escape probability W, but in the variable model at this concentration, 21.2% of the binding sites have an escape probability of W; 22.7%, W^2; 13.0%, W^3; 4.2%, W^4; and 0.7%, W^5. The sensitivity to initial conditions becomes extreme as W decreases. For $W = 0.1$ and 0.2, diffusion is anomalous over all times shown for random initial conditions, and for thermal equilibrium initial conditions, diffusion is similar to diffusion with inert obstacles, but with a much lower diffusion coefficient. The curves are independent of system size because the distribution of binding energies is nonsingular.

In summary, for thermal equilibrium initial conditions, the obstruction/binding model lowers D significantly, more in the variable case than in the uniform case. But binding does not affect anomalous diffusion. The only anomalous diffusion is that which the obstacles produce.

Point binding sites: singular distribution of waiting times

Much work has been published in the physics literature on point binding sites with a singular distribution of waiting times (for example, Harder et al., 1987; Haus and Kehr, 1987). We consider a valley model (Fig. 2 *a*) where the escape probability W is given by a power-law distribution

$$P(W)\mathrm{d}W = (1 - \alpha)W^{-\alpha}\mathrm{d}W, \tag{9}$$

with $0 < \alpha < 1$. The waiting time is $1/W$. The cumulative distribution is

$$F(W) = \int_0^W P(w)\mathrm{d}w = W^{1-\alpha}. \tag{10}$$

To obtain the escape probability for a binding site, we generate a random number R between 0 and 1, and find W from

$$W = R^{1/(1-\alpha)}. \quad (11)$$

Thus, for $\alpha = 0.25$, if $R = 1$, $W = 1$; if $R = 0.1$, $W = 0.0464$; if $R = 0.01$, $W = 0.00215$; and if $R = 0.001$, $W = 0.0001$. Each time R decreases by a factor of 10, W decreases by a factor of $10^{4/3} = 21.5$. This is the recipe for fractal time of Shlesinger (1988): an order of magnitude longer waiting time, an order of magnitude less often (where the orders of magnitude are not necessarily in base 10, or in the same base). This distribution is singular, that is, there is a nonzero probability of obtaining any $W > 0$. If the escape probability is given by an Arrhenius factor $W = \exp(-\beta E)$, this distribution of W corresponds to an exponential distribution of binding energies

$$P(E)dE = (1 - \alpha)\exp[(1 - \alpha)E]dE. \quad (12)$$

For this probability distribution, the effect of the initial condition is large, showing the same pattern as the variable obstruction/binding model in Fig. 3. For random initial conditions, diffusion is anomalous for all times examined. For equilibrium initial conditions, diffusion is normal for all times. For short annealing times, diffusion is normal for short times and anomalous at long times. For long annealing times, diffusion is normal for all times. The approach to equilibrium is very slow. (In an infinite system, there is no thermal equilibrium, but there is an equilibrium state in the finite system used in the Monte Carlo calculations.)

For random initial conditions, in the limit $t \rightarrow \infty$ the anomalous diffusion exponent (Eq. 4) is $d_w = 1/(1 - \alpha)$ (Harder et al., 1987). The approach to this limit is slow, and in practice one must include correction terms (de Alcantara Bonfim and Berrondo, 1989).

Diffusion is anomalous for random initial conditions because the distribution of well depths is singular, so that no matter how deep a well a tracer has already been in, it always has a nonzero probability of falling into a deeper well (Harder et al., 1987). Similarly, in the case of anomalous diffusion due to inert obstacles at the percolation threshold, the self-similarity of the percolation cluster implies that there are geometric traps on all length scales. A tracer may escape from a small dead end only to find that it is still trapped in a larger dead end, a predicament not limited to diffusing particles.

The distribution is singular because diffusion in this model is sensitive to the size of the system. For equilibrium initial conditions in a finite system, diffusion is always normal, but as the system size was increased from 32×32 to 256×256, the diffusion coefficient decreased by a factor of ~4. At fixed lattice size, the fluctuations in diffusion coefficient from run to run are significant. The value of $D^*(C)$ depends strongly on the depth of the deepest wells encountered, and as the system becomes larger, the probable depth of the deepest well increases.

The effect of α is shown in Fig. 6. For random initial conditions, diffusion is anomalous, and for equilibrium initial conditions in a finite system, diffusion is normal. The diffusion coefficient decreases as α increases.

Mountain model: bond diffusion with a distribution of barrier heights

In the mountain model (Fig. 2 *a*), the lattice sites are all at $E = 0$, so the thermal equilibrium distribution is uniform. A high barrier in the mountain model has much less effect than a deep well in the valley model, because in the mountain model a tracer is likely to go around a high barrier (Bunde, 1988). Results are shown in Fig. 7 for two distributions of barrier heights. In Fig. 7 *a* the transition probabilities W are given by the power law distribution (Eq. 9). In Fig. 7 *b* the barrier height E is uniformly distributed on a prescribed interval $(0, E_{MAX})$, and W is obtained from the Arrhenius factor. In both cases, diffusion is slowed, but not as much as in some of the other models. Diffusion is anomalous at short times and normal at long times, but the anomalous diffusion does not disappear at thermal equilibration. The power law distribution of barrier heights used here is the same singular distribution that was used in the previous model, but the effects on diffusion are much less, as a comparison of Figs. 6 and 7 *a* shows. Argyrakis et al. (1995) discuss various aspects of diffusion, including the crossover time, for several distributions of barrier heights.

Continuous-time random walk model

To examine the effect of long-time tails on fluorescence photobleaching recovery, Nagle (1992) used a CTRW model (Scher et al., 1991). Here binding is represented by a waiting time distribution function

$$\psi(t) = \beta/(1 + t)^{1+\beta} \quad (13)$$

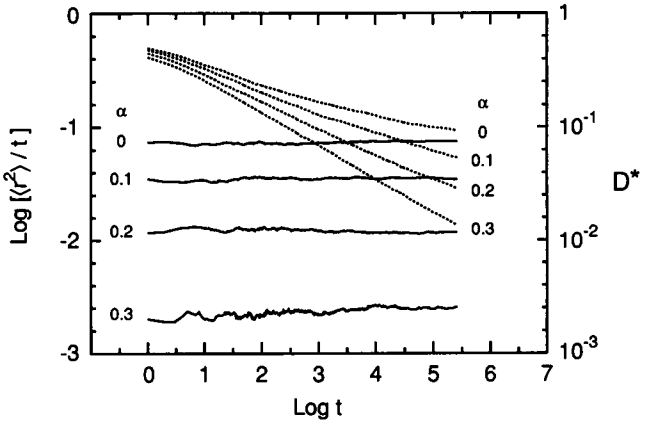

FIGURE 6 Unobstructed binding sites with a singular distribution of escape probabilities. Log[$\langle r^2 \rangle/t$] as a function of log t, for the indicated values of α in Eq. 9. ·····, Random initial conditions. ——, equilibrium initial conditions for a 256×256 system (see text).

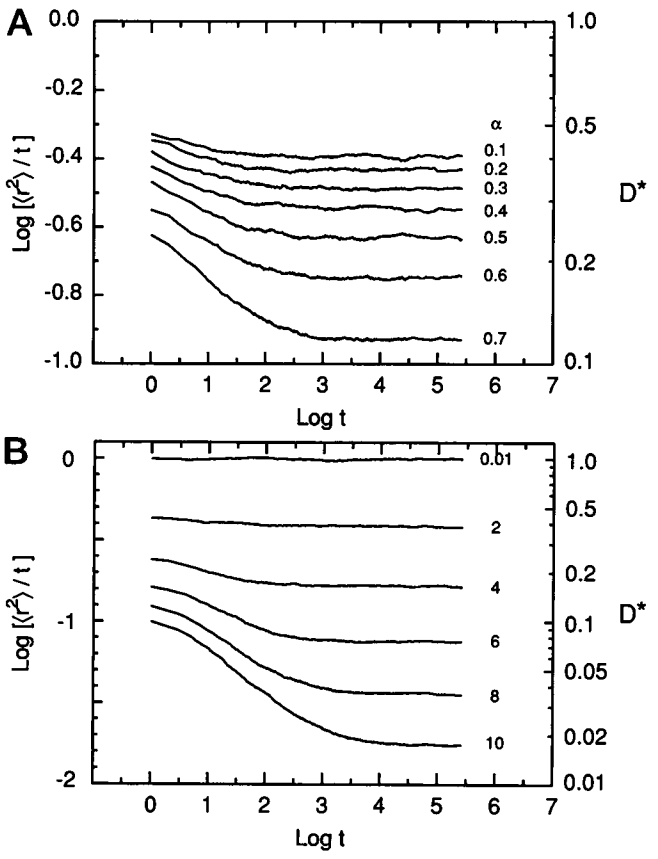

FIGURE 7 Monte Carlo results for $\log[\langle r^2\rangle/t]$ as a function of $\log t$ for two mountain models. (*A*) Power-law distribution of W (Eq. 9) with the indicated values of the parameter α. (*B*) Uniform distribution of barrier heights E on an interval $(0,E_{MAX})$, with $W = \exp(-\beta E)$. Values of E_{MAX} are indicated.

with $\beta > 0$, giving the probability that a tracer that last jumped at $t = 0$ will jump at a time t. Long-time tails result because ψ decays algebraically with t; if ψ decayed exponentially, diffusion would be normal. For an unobstructed system with this distribution function,

$$\langle r^2\rangle \sim t^{\beta} \tag{14}$$

for large t (Blumen et al., 1984) so that from Eq. 4,

$$d_w = 2/\beta. \tag{15}$$

There is an important difference between this model and the others. In the other models, the escape time from a given site is fixed ("quenched disorder"); in the CTRW model, the escape time from a given site varies with time ("annealed disorder"), with a random value given by Eq. 13. There is no thermal equilibration. No moves ever fail; some simply require a long time.

The behavior of this model can be explained by the arguments used earlier. Diffusion is anomalous because a tracer always has a nonzero probability of being trapped for a longer time than it had previously been. Annealing has no effect, and diffusion is independent of system size because the probability of trapping is independent of position. There is temporal disorder but no spatial disorder.

Monte Carlo results are shown in Fig. 8. Diffusion is always anomalous, and the anomalous diffusion exponent is given to high accuracy by Eq. 15 for $0.3 \le \beta \le 0.7$. Note that d_w may be very large. For Nagle's value $\beta = 0.3$, $d_w = 6.67$, so diffusion is much more anomalous than for inert point obstacles, where $2.0 \le d_w \le 2.87$.

Diffusion coefficients

We summarize the results of the different models by plots of the long-range diffusion coefficients for initial conditions of thermal equilibrium.

Approximate values of D^* for the obstruction/binding model can be calculated by assuming that D^* can be written as the product of obstruction and binding terms,

$$D^*(C,\{W\}) = D^*_{OBST}(C)D^*_{BIND}(\{W\}), \tag{16}$$

where D^*_{OBST} is obtained from Monte Carlo calculations for inert obstacles, and D^*_{BIND} is calculated from Eq. 7, which holds for the valley model with thermal equilibrium initial conditions. In the uniform obstruction/binding model on the triangular lattice, if the fraction of free sites among the unblocked sites is f_0 and the fraction of binding sites among the unblocked sites is f_B, then $1/D^*_{BIND} = f_B/W + f_0$. Here $f_0 = (1 - C)^6$ and $f_B = 1 - f_0$, so

$$\frac{1}{D^*_{BIND}} = [1 - (1 - C)^6]\frac{1}{W} + (1 - C)^6. \tag{17}$$

As $W \to 0$, the second term becomes negligible and $D^*_{BIND} \propto W$.

For the uniform obstruction/binding model, Fig. 9 *a* shows the diffusion coefficient as a function of concentration for various escape probabilities. The points are Monte Carlo results and the lines are from Eqs. 16 and 17. Agreement is good except near the percolation threshold, where the values of D^* are less accurate because of the length of the Monte Carlo runs needed to reach the limiting value (see

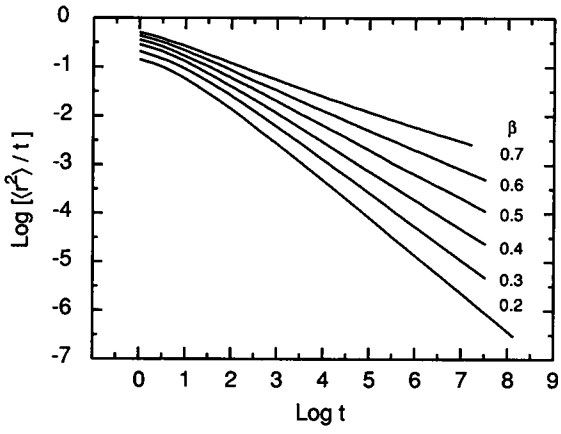

FIGURE 8 Monte Carlo results for $\log[\langle r^2\rangle/t]$ as a function of $\log t$ for the CTRW model with the indicated values of β.

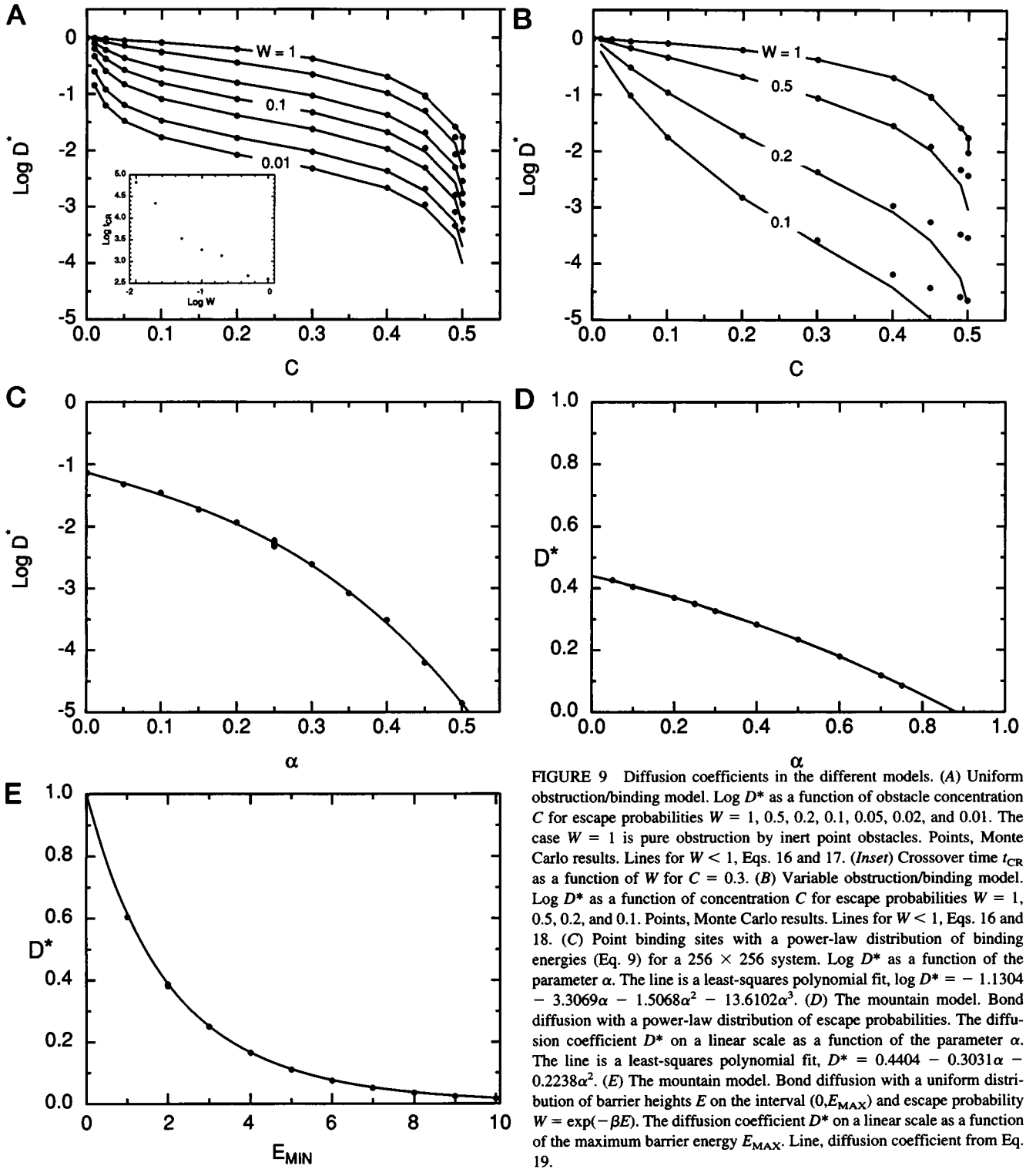

FIGURE 9 Diffusion coefficients in the different models. (*A*) Uniform obstruction/binding model. Log D^* as a function of obstacle concentration C for escape probabilities $W = 1$, 0.5, 0.2, 0.1, 0.05, 0.02, and 0.01. The case $W = 1$ is pure obstruction by inert point obstacles. Points, Monte Carlo results. Lines for $W < 1$, Eqs. 16 and 17. (*Inset*) Crossover time t_{CR} as a function of W for $C = 0.3$. (*B*) Variable obstruction/binding model. Log D^* as a function of concentration C for escape probabilities $W = 1$, 0.5, 0.2, and 0.1. Points, Monte Carlo results. Lines for $W < 1$, Eqs. 16 and 18. (*C*) Point binding sites with a power-law distribution of binding energies (Eq. 9) for a 256 × 256 system. Log D^* as a function of the parameter α. The line is a least-squares polynomial fit, $\log D^* = -1.1304 - 3.3069\alpha - 1.5068\alpha^2 - 13.6102\alpha^3$. (*D*) The mountain model. Bond diffusion with a power-law distribution of escape probabilities. The diffusion coefficient D^* on a linear scale as a function of the parameter α. The line is a least-squares polynomial fit, $D^* = 0.4404 - 0.3031\alpha - 0.2238\alpha^2$. (*E*) The mountain model. Bond diffusion with a uniform distribution of barrier heights E on the interval $(0,E_{MAX})$ and escape probability $W = \exp(-\beta E)$. The diffusion coefficient D^* on a linear scale as a function of the maximum barrier energy E_{MAX}. Line, diffusion coefficient from Eq. 19.

Fig. 1). The crossover time from anomalous to normal diffusion is larger for obstruction/binding models than for inert obstacles, particularly for small W. The inset in Fig. 9 *a* gives a log-log plot of the crossover time t_{CR} as a function of W.

Fig. 9 *b* shows similar results for the variable obstruction/binding model. The diffusion coefficient is much lower, so much so that the calculations were carried out only for $W \geq 0.1$. Again D may be calculated from Eqs. 7 and 16. For this model

$$\frac{1}{D^*_{BIND}} = \frac{1}{1-f_6}\left[\frac{f_0}{1} + \frac{f_1}{W} + \frac{f_2}{W^2} + \frac{f_3}{W^3} + \frac{f_4}{W^4} + \frac{f_5}{W^5}\right]. \quad (18)$$

Here f_i are the fractions of unblocked sites with exactly i nearest-neighbor obstacles, and the factor $1/(1 - f_6)$ is included because the Monte Carlo program excludes isolated sites $i = 6$. The f_i are simply the binomial terms $f_0 = (1 - C)^6$, $f_1 = 6C(1 - C)^5$, ... Again the Monte Carlo results are shown as points and the equations are shown as lines. Away from the percolation threshold, agreement is reasonably good.

Fig. 9 *c* shows the diffusion coefficient as a function of α for a 256 × 256 system of point binding sites with a power law distribution of escape probabilities. All lattice points are binding sites, and the distribution of escape probabilities is singular, so the diffusion coefficients are low. From Eqs. 7 and 9, for $\alpha > 0$,

$$\frac{1}{D^*} = \int_{W_{MIN}}^{1} P(w)dw\frac{1}{w} = \frac{1-\alpha}{\alpha}\left[\frac{1}{W_{MIN}^{\alpha}} - 1\right],$$

which diverges as $W_{MIN} \to 0$, giving $D^* = 0$. That is, for a singular power law distribution in an infinite system there is an arbitrarily deep well, and in thermal equilibrium the tracer will be trapped there. For $\alpha = 0.25$, as the system size L increases from 32 to 256, D^* goes to zero as $1/L^{0.67}$.

In the Monte Carlo calculations for the power law distribution, the system is finite and the well depth is bounded. We can then calculate D^* for the sites actually visited in the random walk

$$\frac{1}{D_V^*} = \sum_{\text{All visits}} \frac{1}{W},$$

which is a good approximation to the observed diffusion coefficient. We can also calculate D^* as a sum over all the lattice sites in the finite system,

$$\frac{1}{D_L^*} = \sum_{\text{All lattice sites}} \frac{1}{W},$$

which is a lower limit for the diffusion coefficient for that configuration of traps. The fact that $D_L^* < D_V^*$ indicates that for the conditions of the calculations, 200 tracers and 256K time steps, the tracers do not sample the 256 × 256 grid completely.

Fig. 9 *d* shows the diffusion coefficient for the mountain model with a power law distribution of escape probabilities, and Fig. 9 *e* shows similar results for a uniform distribution of barrier heights.

The effect on D^* is smaller than in the valley models, small enough that D^* is shown on a linear scale instead of a logarithmic one, because a tracer is likely to avoid high barriers. For a uniform distribution of barrier heights on the interval $(0,E_{MAX})$, D^* is given to good accuracy by an effective-medium equation (Bernasconi, 1973; Ambaye and Kehr, 1995),

$$D^* = \frac{1}{2}\frac{1 - \exp(-2\beta E_{MAX}/3)}{\exp(\beta E_{MAX}/3) - 1}. \quad (19)$$

For the CTRW model, diffusion is always anomalous, and the diffusion coefficient is always time dependent, so no graph of D^* is shown.

Experiments

We discuss results on the LDL receptor in human fibroblasts from fluorescence photobleaching recovery (Barak and Webb, 1982) and single-particle tracking experiments (Ghosh, 1991). We take the tracer size to be the size of LDL, which is a sphere of diameter 22 nm (Ghosh and Webb, 1994). The area of the receptor within the membrane is much smaller than this, because the receptor has a single transmembrane helix (Brown and Goldstein, 1986). We assume an obstacle diameter of 4 nm. Recall that the lattice spacing ℓ is the sum of the diameters of an obstacle and a tracer, so that a pair of adjacent obstacles will just block passage of a tracer between them.

The actual fraction of immobile proteins in a cell membrane is not well known, and not all immobile proteins are necessarily traps. One measure of the obstacle concentration is the immobile fraction in fluorescence photobleaching experiments, summarized by Edidin (1992). Fifty measurements on various proteins and cell types give widely scattered immobile fractions, typically 20% to 70%. As Nagle (1992) pointed out, the fractional recovery can depend on the measurement time. A better approach to evaluating the total immobile fraction was developed by Ryan et al. (1988), who measured the equilibrium spatial distribution of labeled proteins when a spherical cell was subjected to an electric field. This method, which accounts for exclusion by all species, gave an immobile fraction of 30 ± 15%, although this depended on the label used.

For the LDL receptor, the diffusion coefficients from photobleaching are D(cell) = 4.5×10^{-11} cm^2/s in an intact cell and D(bleb) = 1.4×10^{-9} cm^2/s in a bleb, where the proteins are released from cytoskeletal influence (Barak and Webb, 1982). So the diffusion coefficient is reduced by a factor of $D^* = 0.032$ on going from the bleb to the intact cell. This factor is similar to the ratio of the diffusion coefficient of band 3 in normal erythrocytes to that in spherocytes lacking membrane skeletons, $D^* = 0.02$ (Sheetz et al., 1980). We will assume various mechanisms for hindering diffusion, find the obstacle concentration required to reduce the diffusion coefficient by the observed factor, and examine the effect of that obstacle concentration on anomalous diffusion. (To do this, we need Monte Carlo results at that obstacle concentration. We do not rerun the calculation at the exact obstacle concentration, but choose a run for which D^* is close to the observed value.) In this section we distinguish between the dimensionless Monte Carlo crossover time t_{CR}^* and the crossover time in physical units t_{CR}.

First, we assume pure obstruction, with inert random point obstacles on a triangular lattice. To reproduce the observed D^*, we take the obstacle concentration to be C =

0.482, near the percolation threshold $C_P = 0.5$, and find from earlier work (Saxton, 1994) $D^* = 0.0323$, $t_{CR}^* = 1.2 \times 10^6$, and $d_w = 2.70$. So $\langle r^2 \rangle \approx t^{0.74}$ in the region of anomalous diffusion, close to the experimental values (Ghosh, 1991). To convert to physical units, we use $D_0 = D$(bleb) and $\ell = 26$ nm to get $\tau = 1.21$ ms. Then $t_{CR} = \tau t_{CR}^* = 24$ min. The single-particle tracking trajectories were 5 min long (Ghosh, 1991), and the longest photobleaching measurements were 11.3 min (Barak and Webb, 1982), so both experiments would see only anomalous diffusion. A modified equation for photobleaching recovery (Feder, 1993) would then apply. Her treatment assumes that there is no crossover and leads to an equation of the usual form but with a nonintegral power of time replacing the time. The difficulty with interpreting the experimental results in terms of simple obstruction is that episodes of apparently directed motion were also observed (Ghosh, 1991; Anderson et al., 1992). It seems unlikely that directed motion could occur in a system of randomly distributed obstacles so close to the percolation threshold, unless the directed and diffusive motions occurred in distinct domains with different obstacle concentrations.

In fact, the tracers are larger than the obstacles. If we go through the same calculations assuming inert point obstacles and hexagonal tracers of unit radius (Saxton, 1993a), we find that the obstacle concentration required to give $D^* = 0.032$ is $C = 0.11$, close to the percolation threshold $C_P = 0.1156$. The crossover time and the anomalous diffusion exponent are similar to those for point obstacles and tracers.

Next, we consider the effect of trapping. In the case of inert obstacles, the conversion factor $\tau = \ell^2/4D_0$ between Monte Carlo and physical units is simply the time required for a tracer to diffuse one lattice constant in the absence of obstacles. In the case of obstruction with binding, τ is the time required for the tracer to diffuse one lattice constant in the presence of binding but not obstacles, so we calculate τ using $D_0 = D(\text{cell})/D^*_{OBST}(C)$. We thus assume that binding slows diffusion uniformly and that the obstacles alone are responsible for the anomalous diffusion. Another way to think of this is that distance, not time, is fundamental. The crossover is a geometric property of the obstacles, so a tracer has to diffuse a certain distance to see the crossover, and when binding occurs the tracer takes a longer time to diffuse that distance.

Assume the uniform obstruction/binding model with $C = 0.3$ and $W = 0.1$. Then from Fig. 9 *a*, $D^* = 0.0475$, in the same range as the observed value. From Fig. 9 *b*, $D^*_{OBST} = 0.424$ and from Eq. 17, $D^*_{BIND} = 0.112$. From Fig. 4 *b*, $t_{CR}^* = 2500$ and $d_w = 2.22$, so that $\langle r^2 \rangle \approx t^{0.9}$ in the region of anomalous diffusion. To convert to physical units, we again use $\ell = 26$ nm, but we use $D(\text{cell})/D^*_{OBST}$ as D_0, and obtain $\tau = 15.9$ ms and a crossover time $t_{CR} = 40$ s. Here binding lowers the obstacle concentration required to reproduce the observed diffusion coefficient. Diffusion is therefore less anomalous, but the crossover time is shortened to the point where it could be detectable in the photobleaching and tracking experiments.

Finally, we consider hydrodynamic interactions. The hydrodynamic interaction between immobile obstacles and mobile tracers can reduce the diffusion coefficient significantly (Bussell et al., 1995; Dodd et al., 1995). But this interaction might not be important here because the LDL receptor has only a single transmembrane helix and is therefore too small for a hydrodynamic treatment.

To see what might happen, we consider a fictitious system in which the tracers and obstacles are both hexagons of unit radius. Let the obstacle concentration be 0.15. From figure 2 of Bussell et al. (1995), $D^*_{HYDRO} = 0.07$, and from figure 1 *b* of Saxton (1993a), $D^*_{OBST} = 0.42$, giving $D^* = 0.029$. From a plot of Monte Carlo results, $t_{CR}^* = 2500$ and $d_w = 2.27$, so that in the region of anomalous diffusion $\langle r^2 \rangle \approx t^{0.88}$. Given the particle size, we can then find τ, again using $D(\text{cell})/D^*_{OBST}$ as D_0, and convert the crossover time to physical units.

Just as in the case of trapping, the hydrodynamic interaction lowers the obstacle concentration needed to give the experimental diffusion coefficient, so that diffusion is less anomalous. It will be very interesting to see whether the hydrodynamic interactions themselves lead to anomalous diffusion, and whether there is a hydrodynamic interaction with membrane proteins that have a single transmembrane segment.

DISCUSSION

We have examined anomalous diffusion in a variety of models of obstruction and binding, and reviewed some principles needed to understand the behavior of a diffusing particle: the distinction between mountain and valley models, the importance of the initial conditions in determining whether diffusion is anomalous or normal, and the distinction between singular and nonsingular distributions of binding energies.

For valley models with random initial conditions—a nonequilibrium state—diffusion is highly anomalous over a significant time range. But for valley models in a thermal equilibrium initial state, the behavior is much different. In models without obstacles, no anomalous diffusion occurs at any time. In models with obstacles, diffusion is anomalous only to the extent required by the obstacles. So a large class of binding models does not produce anomalous diffusion, and binding in the obstruction/binding model does not enhance anomalous diffusion. The two versions of the mountain model yield anomalous diffusion with a small to moderate decrease in the diffusion coefficient, but the anomalous diffusion is not destroyed by thermal equilibration. The CTRW model used by Nagle (1992) produces highly anomalous diffusion over all times. This model is an extreme case, so that experimental observation of the behavior predicted by the CTRW model would place strong constraints on the mechanisms hindering diffusion.

Binding can give much lower diffusion coefficients than pure obstruction can. Binding with thermal equilibrium

initial conditions does not lead to diffusion that is more anomalous (larger d_w), but it increases the observed crossover time from normal to anomalous diffusion by lowering the diffusion coefficient.

In ideal fluorescence photobleaching recovery experiments, the interaction of the tracer with other species in the membrane is unchanged by the presence of the label, unbleached or bleached. Similarly, an ideal label in single-particle tracking experiments has no effect on the tracer or its interactions. The initial condition will then be thermal equilibrium, unless the labeling and measurement are very rapid. In nonideal labeling, interactions of the tracer with other species are different for bleached and unbleached label, and a short photobleaching pulse could produce a nonequilibrium initial condition.

In the obstruction/binding model with an ideal label, then, a photobleaching measurement with binding would look like a photobleaching measurement without binding, except that the diffusion coefficient would be lower. But in a single-particle tracking experiment, binding can be detected by measuring waiting times in very small (single-pixel) regions. These data can be analyzed by using an expression for the probability that a random walk will remain in a circle of prescribed radius for a given time (Saxton, 1993b). A useful method of carrying out this analysis is given by Simson et al. (1995).

In the Monte Carlo calculations for binding, the results are sensitive to the annealing time, but for pure obstruction, the results are independent of annealing time. What this implies is that the experimental clocks in obstruction and binding are much different. For binding, the clock starts when the tracer and the binding sites are first physically mixed, but for obstruction the clock starts every time a measurement is begun.

A key observation for distinguishing mechanisms producing anomalous diffusion in cell membranes would be detection of a crossover from anomalous to normal diffusion. Further work is needed to determine the conditions under which the crossover can be observed in single-particle tracking experiments. Further work is also required to examine trapping models not considered here, such as the long-range model of Fig. 2 *c*.

A singular distribution of binding energies yields a strong dependence on the system size, and D decreases as the system size increases. On the contrary, fluorescence photobleaching recovery experiments on cell membranes (Yechiel and Edidin, 1987; Edidin and Stroynowski, 1991; Edidin et al., 1994) found that D increases as the bleach spot size increases. The experimental results were explained by Schram et al. (1994), who assumed that recovery occurs in small domains at the edge of the photobleached region. To examine photobleaching in the presence of traps, it would be useful to combine and extend the models of Schram et al. (1994) and of Nagle (1992). Note that tracers in deep wells would act as obstacles or as slowly recovering fluorescent components, depending on the ratio of the waiting time to the photobleaching recovery time. This behavior is approximated by the CTRW model. Note also that varying the spot size varies not only the system size but also the photobleaching recovery time (Edidin et al., 1994).

I thank Paulo Almeida, Ken Jacobson, John Nagle, and Watt Webb for helpful discussions; Rudi Simson for a copy of his thesis; and the reviewers for useful suggestions.

This work was supported by National Institutes of Health grant GM38133.

REFERENCES

Ambaye, H., and K. W. Kehr. 1995. Asymptotic diffusion coefficient of particles in a random medium. *Phys. Rev. E.* 51:5101–5102.

Anderson, C. M., G. N. Georgiou, I. E. G. Morrison, G. V. W. Stevenson, and R. J. Cherry. 1992. Tracking of cell surface receptors by fluorescence digital imaging microscopy using a charge-coupled device camera. Low-density lipoprotein and influenza virus receptor mobility at 4°C. *J. Cell Sci.* 101:415–425.

Argyrakis, P., A. Milchev, V. Pereyra, and K. W. Kehr. 1995. Dependence of the diffusion coefficient on the energy distribution of random barriers. *Phys. Rev. E.* 52:3623–3631.

Barak, L. S., and W. W. Webb. 1982. Diffusion of low density lipoprotein-receptor complex on human fibroblasts. *J. Cell Biol.* 95:846–852.

Bernasconi, J. 1973. Electrical conductivity in disordered systems. *Phys. Rev. B.* 7:2252–2260.

Binder, K., and D. W. Heermann. 1992. Monte Carlo Simulation in Statistical Physics: An Introduction, 2nd ed. Springer-Verlag, Berlin.

Blumen, A., J. Klafter, B. S. White, and G. Zumofen. 1984. Continuous-time random walks on fractals. *Phys. Rev. Lett.* 53:1301–1304.

Bouchaud, J.-P., and A. Georges. 1988. The physical mechanisms of anomalous diffusion. *In* Disorder and Mixing. E. Guyon, J.-P. Nadal, and Y. Pomeau, editors. Kluwer Academic Publishers, Dordrecht. 19–29.

Bouchaud, J.-P., and A. Georges. 1990. Anomalous diffusion in disordered media: statistical mechanisms, models and physical applications. *Phys. Rep.* 195:127–293.

Brown, M. S., and J. L. Goldstein. 1986. A receptor-mediated pathway for cholesterol homeostasis. *Science.* 232:34–47.

Brust-Mascher, I., T. J. Feder, J. P. Slattery, B. Baird, and W. W. Webb. 1993. FPR data on mobility of cell surface proteins reevaluated in terms of temporally constrained molecular motions. *Biophys. J.* 64:354*a*. (Abstr.)

Bunde, A. 1988. Anomalous transport in disordered media. Solid State Ionics. 28–30:34–40.

Bussell, S. J., D. L. Koch, and D. A. Hammer. 1995. Effect of hydrodynamic interactions on the diffusion of integral membrane proteins: diffusion in plasma membranes. *Biophys. J.* 68:1836–1849.

de Alcantara Bonfim, O. F., and M. Berrondo. 1989. Corrections to scaling for diffusion in disordered media. *J. Phys. A.* 22:4673–4679.

Dodd, T. L., D. A. Hammer, A. S. Sangani, and D. L. Koch. 1995. Numerical simulations of the effect of hydrodynamic interactions on diffusivities of integral membrane proteins. *J. Fluid. Mech.* 293: 147–180.

Edidin, M. 1992. Translational diffusion of membrane proteins. *In* The Structure of Biological Membranes. P. Yeagle, editor. CRC Press, Boca Raton, FL. 539–572.

Edidin, M., and I. Stroynowski. 1991. Differences between the lateral organization of conventional and inositol phospholipid-anchored membrane proteins. A further definition of micrometer-scale membrane domains. *J. Cell Biol.* 112:1143–1150.

Edidin, M., M. C. Zúñiga, and M. P. Sheetz. 1994. Truncation mutants define and locate cytoplasmic barriers to lateral mobility of membrane glycoproteins. *Proc. Natl. Acad. Sci. USA.* 91:3378–3382.

Feder, T. J. 1993. Fluorescence studies of structural, dynamic and functional properties of the rat basophilic leukemia cell membrane. Ph.D. thesis. Cornell University. 136 pp.

Ghosh, R. N. 1991. Mobility and clustering of individual low-density lipoprotein receptor molecules on the surface of human skin fibroblasts. Ph.D. thesis. Cornell University. 260 pp.

Ghosh, R. N., and W. W. Webb. 1994. Automated detection and tracking of individual and clustered cell surface low density lipoprotein receptor molecules. *Biophys. J.* 66:1301–1318.

Harder, H., S. Havlin, and A. Bunde. 1987. Diffusion on fractals with singular waiting-time distribution. *Phys. Rev. B.* 36:3874–3879.

Haus, J. W., and K. W. Kehr. 1987. Diffusion in regular and disordered lattices. *Phys. Rep.* 150:263–406.

Havlin, S., and D. Ben-Avraham. 1987. Diffusion in disordered media. *Adv. Phys.* 36:695–798.

Hill, T. H. 1985. Cooperativity Theory in Biochemistry: Steady-State and Equilibrium Systems. Springer-Verlag, New York. 14–22.

Jiang, X.-P., and H. Metiu. 1988. A Monte Carlo analysis of diffusion measurements in surface science systems that undergo phase transitions. *J. Chem. Phys.* 88:1891–1900.

Kang, H. C., and W. H. Weinberg. 1992. Dynamic Monte Carlo simulations of surface-rate processes. *Accounts Chem. Res.* 25:253–259.

Limoge, Y., and J. L. Bocquet. 1991. Random walk in amorphous materials. *Mod. Phys. Lett. B.* 5:799–803.

Lindenberg, K., B. J. West, and R. Kopelman. 1989. Diffusion-limited $A + B \rightarrow 0$ reaction: spontaneous segregation. *In* Noise and Chaos in Nonlinear Dynamical Systems. F. Moss, L. Lugiato, and W. Schleich, editors. Cambridge University Press, Cambridge. 142–171.

Lindenberg, K., B. J. West, and R. Kopelman. 1990. Diffusion-limited $A + B \rightarrow 0$ reaction: correlated initial condition. *Phys. Rev. A.* 42:890–894.

Mak, C. H., H. C. Andersen, and S. M. George. 1988. Monte Carlo studies of diffusion on inhomogeneous surfaces. *J. Chem. Phys.* 88:4052–4061.

Nagle, J. F. 1992. Long-tail kinetics in biophysics? *Biophys. J.* 63:366–370.

Parris, P. E., and B. D. Bookout. 1993. Trapping-to-percolation transition in the hopping diffusion of substitutionally disordered solids with a binary energy distribution. *Phys. Rev. B.* 47:562–565.

Ryan, T. A., J. Myers, D. Holowka, B. Baird, and W. W. Webb. 1988. Molecular crowding on the cell surface. *Science.* 239:61–64.

Saxton, M. J. 1987. Lateral diffusion in an archipelago: the effect of mobile obstacles. *Biophys. J.* 52:989–997.

Saxton, M. J. 1992. Lateral diffusion and aggregation: a Monte Carlo study. *Biophys. J.* 61:119–128.

Saxton, M. J. 1993a. Lateral diffusion in an archipelago: dependence on tracer size. *Biophys. J.* 64:1053–1062.

Saxton, M. J. 1993b. Lateral diffusion in an archipelago: single-particle diffusion. *Biophys. J.* 64:1766–1780.

Saxton, M. J. 1994. Anomalous diffusion due to obstacles: a Monte Carlo study. *Biophys. J.* 66:394–401.

Scalettar, B. A., and J. R. Abney. 1991. Molecular crowding and protein diffusion in biological membranes. *Comments Mol. Cell. Biophys.* 7:79–107.

Scher, H., M. F. Shlesinger, and J. T. Bendler. 1991. Time-scale invariance in transport and relaxation. *Phys. Today.* 44(1):26–34.

Schram, V., J.-F. Tocanne, and A. Lopez. 1994. Influence of obstacles on lipid lateral diffusion: computer simulation of FRAP experiments and application to proteoliposomes and biomembranes. *Eur. Biophys. J.* 23:337–348.

Sheetz, M. P., M. Schindler, and D. E. Koppel. 1980. Lateral mobility of integral membrane proteins is increased in spherocytic erythrocytes. *Nature.* 285:510–512.

Shlesinger, M. F. 1988. Fractal time in condensed matter. *Annu. Rev. Phys. Chem.* 39:269–290.

Simson, R. 1994. Different modes of lateral mobility for neural cell adhesion molecules as observed by nanovid microscopy and single particle tracking. Diplomarbeit. Technische Universität München. 78 pp.

Simson, R., E. D. Sheets, and K. Jacobson. 1995. Detection of temporary lateral confinement of membrane proteins using single-particle tracking analysis. *Biophys. J.* 69:989–993.

Yechiel, E., and M. Edidin. 1987. Micrometer-scale domains in fibroblast plasma membranes. *J. Cell Biol.* 105:755–760.

Zhang, F., G. M. Lee, and K. Jacobson. 1993. Protein lateral mobility as a reflection of membrane microstructure. *Bioessays.* 15:579–588.